Journal of Materials Chemistry C

ROYAL SOCIETY OF CHEMISTRY

PAPER

View Article Online
View Journal | View Issue

Cite this: J. Mater. Chem. C, 2025, 13, 20571

Prediction of high-temperature superconductivity in LaH_4 at low pressures

Christopher Renskers,[a] Catalin D. Spataru,[b] Marios Zacharias,[cd] Sakun Duwal,[e] Timothy Elmslie,[e] Peter A. Sharma[e] and Elena R. Margine *[a]

Received 7th July 2025,
Accepted 7th September 2025

DOI: 10.1039/d5tc02600h

rsc.li/materials-c

Superconducting hydrides have received significant attention in the last decade due to their potential for room-temperature superconductivity. However, achieving high critical temperatures (T_cs) typically requires extreme pressures exceeding 150 GPa. Recently, a new, low-pressure $R\bar{3}m$-LaH_4 phase was observed to form above approximately 20 GPa. Here, we perform first-principles calculations to investigate the electron–phonon interactions and superconducting properties of the new phase across a range of pressures. At the harmonic level, the system is found to be dynamically unstable, but this is remedied through the inclusion of anharmonic effects. We estimate that T_c reaches up to 115 K at 25 GPa, driven by a high density of states at the Fermi level (N_F) and soft phonon modes. However, superconductivity is suppressed with increasing pressure, as T_c rapidly decreases to 34 K at 60 GPa and 11 K at 100 GPa, due to a reduction in N_F and phonon hardening.

1 Introduction

Room-temperature superconductivity has long been a highly sought after goal in materials science. The discovery of superconductivity in H_3S at 203 K and 155 GPa[1] marked a pivotal breakthrough, demonstrating that high-T_c superconductivity could be realized in hydrogen-rich systems under pressure. This was soon followed by the realization of near-room-temperature superconductivity in LaH_{10} at 250 K and 170 GPa,[2,3] firmly establishing binary hydrides as front-runners in the search for high-T_c materials. Yttrium hydrides, such as YH_6 and YH_9, have since been both predicted and experimentally confirmed to reach T_c values above 240 K at megabar pressures.[4,5] Other binary hydrides have been experimentally reported to exhibit superconductivity, including CaH_6 (215 K at 172 GPa),[6,7] CeH_9 (100 K at 100 GPa),[8–10] and ThH_{10} (161 K at 175 GPa).[11] These findings demonstrate that binary hydrides have a strong potential to achieve high-T_c, particularly when the hydrogen fraction in a compound exceeds 0.6.[12] The high phonon frequencies of hydrogen and the lower frequency modes from the heavier ions both couple strongly to result in significant electron–phonon (e–ph) coupling, and, therefore, T_c. Although these superhydrides significantly reduce the pressure needed to dissociate molecular H_2 by providing a lattice structure that "chemically pre-compresses" the hydrogen,[13] the required pressures remain prohibitively high for practical applications.

Among binary hydrides, significant research has focused on the lanthanum hydrides following the report of superconductivity in LaH_{10}.[2,3,14–27] In this case, studies have demonstrated strong e-ph coupling,[20] stability at lower pressures,[17] and the importance of anharmonic corrections for achieving dynamical stability.[18] Recently, several lanthanum hydrides with different La : H ratios have been successfully synthesized in the pressure range of 50 to 180 GPa,[28] with the cubic La_4H_{23} phase shown to exhibit superconductivity with a maximum T_c of 105 K at 118 GPa.[29,30]

Building on these results and motivated by the need to identify hydrogen-rich compounds that can achieve high-T_c superconductivity at lower pressures, some of the present authors investigated the formation of La hydrides in cryomilled elemental lanthanum exposed to ammonia borane[31]. Structural evolution under pressures up to 60 GPa revealed a distortion from the $Fm\bar{3}m$ phase to an $R\bar{3}m$ phase, with the new rhombohedral structure becoming kinetically stable at pressures above approximately 20 GPa. Using the observed excess cell volume and comparison with the equation of state calculated *via* density functional theory (DFT) for various lanthanum hydrides, the stoichiometry of the $R\bar{3}m$ phase was determined to correspond to LaH_x with $x \sim 4$.[31]

Based on these experimental observations, we perform first-principles calculations to investigate the superconducting properties of the rhombohedral LaH_4 structure shown in Fig. 1.

[a] Department of Physics, Applied Physics, and Astronomy, Binghamton University-SUNY, Binghamton, New York 13902, USA. E-mail: rmargine@binghamton.edu
[b] Sandia National Laboratories, Livermore, California 94550, USA
[c] Univ Rennes, INSA Rennes, CNRS, Institut FOTON-UMR 6082, Rennes F-35000, France
[d] Computation-based Science and Technology Research Center, The Cyprus Institute, Aglantzia 2121, Nicosia, Cyprus
[e] Sandia National Laboratories, Albuquerque, New Mexico 87185, USA

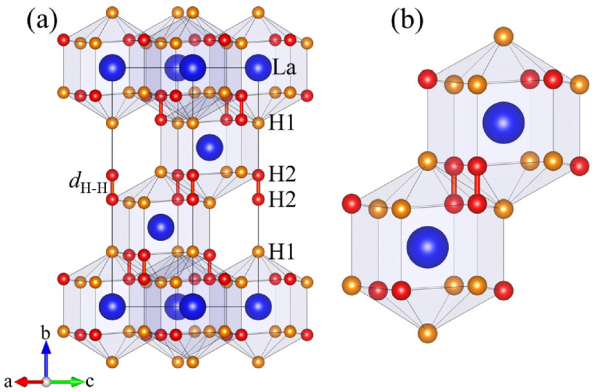

Fig. 1 Crystal structure of $R\bar{3}m$-LaH_4 at 25 GPa. The two nonequivalent hydrogen atoms are labeled as H1 and H2 and the shortest H–H distance is indicated as d_{H-H}. The figures were generated with VESTA.[47]

Our calculations predict a T_c reaching 115 K at 25 GPa, nearly half that of LaH_{10}[15,19] and comparable to La_4H_{23},[29] but at significantly lower pressures. For instance, a tetragonal LaH_4 phase was previously predicted to exhibit a T_c of only 10 K at 300 GPa.[15] Our findings reinforce the potential of the lanthanum hydride family for the development of high-temperature superconducting materials at low to ambient pressures.

2 Methods

First principle calculations were carried out with the Quantum ESPRESSO (QE) package.[32,33] We employed optimized norm-conversing Vanderbilt pseudopotentials (ONCVPSP)[34] from the Pseudo Dojo library[35] generated with the scalar-relativistic revised Perdew–Burke–Ernzerhof (PBEsol) parametrization.[36] A plane wave kinetic-energy cutoff of 120 Ry for the wavefunctions, and 480 Ry for the charge density and potential, were used. For the Brillouin-zone integration of the 5-atom unit cell, we used a Γ-centered $12 \times 12 \times 12$ **k**-mesh[37] with a Methfessel–Paxton[38] smearing of 0.02 Ry. The atomic positions and lattice parameters were optimized until the total energy was converged within 10^{-6} Ry and the force on each atom was less than 10^{-4} Ry Å^{-1}. The dynamical matrices and the linear variation of the self-consistent potential were first computed using density-functional perturbation theory (DFPT)[39] on the irreducible set of a regular $6 \times 6 \times 6$ **q**-mesh.

The force constants computed by DFPT were used as a starting point to calculate phonon anharmonicity *via* the anharmonic special displacement method (ASDM)[40–42] within the framework of the self-consistent phonon theory.[43] The ASDM is used as implemented in the Zacharias–Giustino (ZG) code of the EPW package.[44] For our ASDM calculations, we employed finite differences of amplitude 0.2 Å to iteratively compute the interatomic force constants of ZG configurations at 300 K in $2 \times 2 \times 2$ supercells. We find that such large displacements in low-symmetry systems involving light-mass atoms improve numerical stability and provide a better representation of the anharmonic behavior, particularly for capturing higher-order contributions to the effective force constants. In contrast to high-symmetry hydrides, such as the $Im\bar{3}m$ phase of H_3S, where small 0.01 Å displacements work effectively,[45] such small displacement values lead to phonon instabilities in the soft-mode regions near Γ, as shown in Fig. S1.[46] With the aid of iterative mixing,[42] the convergence of the interatomic force constants was achieved at the 10th iteration, where three successive iterations showed little, to no, change in the anharmonic phonon dispersion. The converged anharmonic force constants were then used to construct the dynamical matrix *via* standard Fourier interpolation on a $6 \times 6 \times 6$ **q**-mesh.

The EPW[44,48–50] code was employed to investigate the e–ph interactions and superconducting properties. The electronic wavefunctions required for the Wannier–Fourier interpolation[51,52] were calculated on a Γ-centered $12 \times 12 \times 12$ **k**-mesh. Nine maximally localized Wannier functions (five d orbitals for La and one s orbital for each H) were used to describe the electronic structure. The anisotropic full-bandwidth Migdal–Eliashberg equations[44,53] were solved with a sparse intermediate representation of the Matsubara frequencies[54] on fine uniform $80 \times 80 \times 80$ **k**- and $40 \times 40 \times 40$ **q**-grids with an energy window of $\pm$ 0.2 eV around the Fermi level. The semiempirical Coulomb parameter, μ^*, was varied from 0.1–0.2.

3 Results and discussion

Guided by experiments, we consider the $R\bar{3}m$ rhombohedral phase (space group no. 166) for the LaH_4 structure. Fig. 2(a) shows our X-ray Diffraction (XRD) results for cryomilled La mixed with ammonia borane, measured in a diamond anvil cell at a pressure of 29.1 GPa. The XRD data reveal the co-existence of $R\bar{3}m$ and FCC La-hydride phases. Fig. 2(b) shows the cell volume of La-hydride inferred from XRD data as a function of pressure. The experimental cell volume is systemically larger than that of the FCC LaH_3 phase over the investigated pressure range.

Utilizing the experimentally determined unit cell and positions of the La atoms, the positions of the H atoms were derived in ref. 31 based on symmetry considerations and atomic relaxation using DFT. The enthalpy of the predicted rhombohedral $R\bar{3}m$ LaH_4 structure was found to be lower by about 0.2 eV f.u.$^{-1}$ than that of several alternative, symmetry-broken LaH_4 configurations obtained *via ab initio* molecular dynamics followed by atomic relaxation. On the other hand, the $I4/mmm$ proposed in ref. 15 remains thermodynamically more favorable than the $R\bar{3}m$ phase in the considered pressure range, as shown in Fig. S2.[46] While the $R\bar{3}m$ phase is not the thermodynamic ground state, our theoretical calculations (including anharmonic effects) indicate that it is dynamically stable, meaning it is kinetically stable in the limit of low temperature. Our experimental data corroborate this, suggesting that the $R\bar{3}m$ phase is observable (thermodynamically metastable) at room temperature. This indicates that it is even more likely to be observable (kinetically stabilized) at low temperatures, particularly near the predicted transition temperature T_c. A similar kinetics-based stabilization mechanism has been shown to overcome the highly unfavorable thermodynamics of Alane at room temperature.[55]

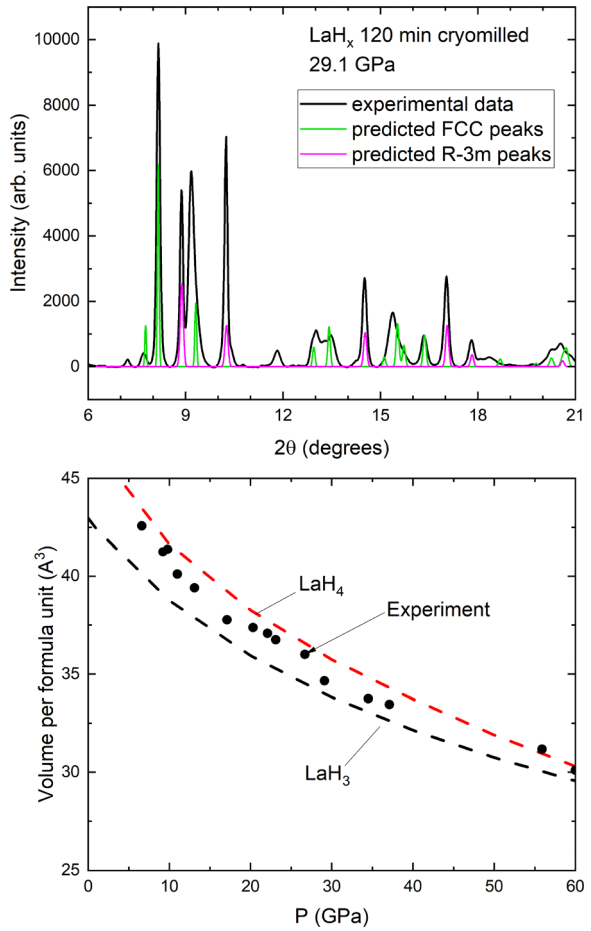

Fig. 2 (a) Powder X-ray diffraction data for cryomilled La mixed with ammonia borane, showing the co-existence of $R\bar{3}m$ and FCC La-hydride phases under high pressure (29.1 GPa). (b) The cell volume of the La-hydride phase inferred from X-ray diffraction data as a function of pressure. DFT simulations of the equation of state are shown for the proposed $R\bar{3}m$ LaH_4 phase and the FCC LaH_3 phase, as indicated. The data presented in this figure are from ref. 31.

The $R\bar{3}m$-LaH_4 phase is predicted to adopt a clathrate structure that is characteristic of other high-temperature superconducting hydrides.[7,18,56–63] The structure consists of a La atom occupying the 3a (0, 0, 0) Wyckoff site and two nonequivalent H atoms, labeled as H1 and H2, located at 6c (0, 0, z_1) and 6c (1/3, 2/3, z_2) Wyckoff sites. The calculated structural parameters at 25, 60, and 100 GPa are provided in Table 1. Each La atom is enclosed in a cage formed by 14 H atoms, as seen in Fig. 1. This matches the crystal structure of $R\bar{3}m$-TeH_4 predicted to stabilize above 230 GPa and reach a T_c of about 70 K.[64] The H-hexagonal rings are slightly buckled at 25 GPa (~0.1 Å) but, as in $R\bar{3}m$-TeH_4, become nearly flat at higher pressures. The H1 atoms form a H_2 unit as marked by the red bond in Fig. 1. This bond marks the shortest H–H distance in the structure, with a value d_{H-H} of 0.96, 0.92, and 0.88 Å for 25, 60, and 100 GPa, respectively. These bond length values are close to the H–H distance of 1 Å predicted for metallic hydrogen near 500 GPa[65] and 0.86 Å for TeH_4 at 300 GPa,[64] but slightly smaller than 1.1 Å for LaH_{10} in the 150–300 GPa pressure range[15,66] and 1.3 Å for La_4H_{23} at 118 GPa.[29]

Table 1 Calculated lattice parameters, shortest H–H distance, and atomic coordinates for the conventional cell of LaH_4 at 25, 60, and 100 GPa. The structure adopts the $R\bar{3}m$ space group with $\gamma = 120°$ at all pressures

Pressure (GPa)	$a = b$ (Å)	c (Å)	d_{H-H} (Å)	Atomic coordinates (fractional)				
25	3.54	9.87	0.96	La	(3a)	0.000	0.000	0.000
				H1	(6c)	0.000	0.000	0.231
				H2	(6c)	0.333	0.666	0.217
60	3.20	9.89	0.92	La	(3a)	0.000	0.000	0.000
				H1	(6c)	0.000	0.000	0.215
				H2	(6c)	0.333	0.666	0.213
100	2.99	9.78	0.88	La	(3a)	0.000	0.000	0.000
				H1	(6c)	0.000	0.000	0.209
				H2	(6c)	0.333	0.666	0.212

The electronic band structure and density of state (DOS) plots in Fig. 3 indicate that the $R\bar{3}m$-LaH_4 phase is metallic across all investigated pressures. The DOS at the Fermi level (N_F) comes from a combination of La and H states with La boasting about 50%, 68%, and 81% increase over H states at 25, 60, and 100 GPa. For hydrogen, the unit formed by the vertically adjacent H2 atoms, as seen in Fig. 1, account for the bulk of the hydrogen states at the Fermi level, contributing 86%, 82%, and 81% of the total hydrogen states at the Fermi level, as depicted in the second panel of Fig. 3. At 25 GPa, N_F reaches its highest value of 0.81 states per eV f.u.$^{-1}$, comparable to values reported

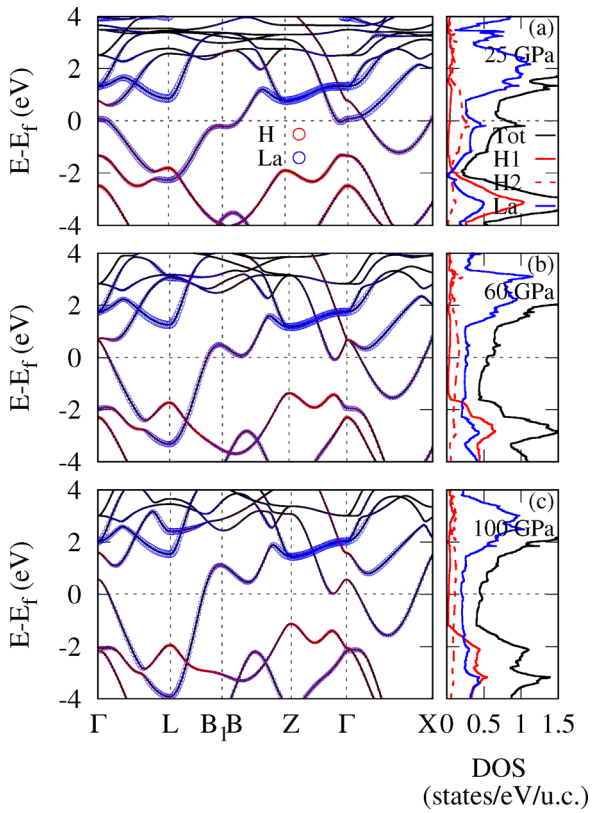

Fig. 3 Electronic band structure with orbital characters, and total and projected density of states (DOS) of LaH_4 at (a)–(c) 25, 60, and 100 GPa. The orbital character is shown in red for H and blue for La states. The total DOS is shown in black, while the projected DOS corresponding to H1, H2, and La atoms are shown with red, dashed red, and blue lines, respectively.

for other high-T_c La–H phases (*e.g.*, ∼ 0.93 states per eV f.u.$^{-1}$ for LaH_{10} at 150 GPa[18] and 0.79 states per eV per La for La_4H_{23} at 120 GPa[29]). This high DOS is largely attributed to a flat electronic band around the Γ point. Furthermore, approximately 0.2 eV below the Fermi level, a Van-Hove-like singularity emerges due to another flat band along the L-B_1 and B-Z high-symmetry directions. The presence of these dispersionless bands at 25 GPa induces a significant variation in the DOS in the vicinity of E_F that is captured by the full-bandwidth approach used to solve the superconducting Migdal–Eliashberg equations.[53] At higher pressures, the flat bands evolve into parabolic dispersions, resulting in a marked decrease in N_F by approximately 33% at 60 GPa and 46% at 100 GPa, respectively. To note, the effect of spin–orbit coupling on the electronic structure was considered and found to be negligible, as shown in Fig. S3.[46]

To further analyze the electronic structure, we calculated the charge density difference between the LaH_4 structure and the sum of its constituent atoms at 25 and 100 GPa. As shown in Fig. 4(a) and (b), there is a buildup of charge on the hydrogen atoms, but, surprisingly, no charge depletion around the La atoms. This suggests minimal to no charge transfer between La and H atoms. Meanwhile, charge depletion is observed between two vertically adjacent H2 atoms, becoming significantly more pronounced at 100 GPa. This trend indicates the formation of H_2 units at higher pressure, resembling molecular hydrogen. This picture is further supported by the electron localization function (ELF) plots in Fig. 4(c) and (d), taken along the (1 1 0) and (0 0 1) planes. Panel (c) reveals the formation of H_2 units between adjacent H2 atoms, as well as the repulsion between La and H1 atoms, which gives rise to the teardrop-shaped features around the H1 atoms. Panel (d) illustrates how the H atoms arrange into a hexagonal ring surrounding the La atom, highlighting the structural characteristics of $R\bar{3}m$-LaH_4.

Fig. 5 presents the vibrational properties of LaH_4. At the harmonic level, depicted by the solid gray lines, the structure exhibits dynamic instabilities across all investigated pressures, with the most pronounced negative phonon modes observed at 25 GPa. This behavior is common among many superconducting hydrides and is typically resolved by accounting for quantum anharmonic effects.[18,68–71] When applying the ASDM, these instabilities are eliminated, as shown by the solid black lines. Notably, the low-frequency La modes at 25 GPa undergo significant renormalization under the ASDM, which has important implications for the superconducting properties of the material.

The phonon dispersion displays a distinct separation between modes associated with lanthanum and hydrogen.

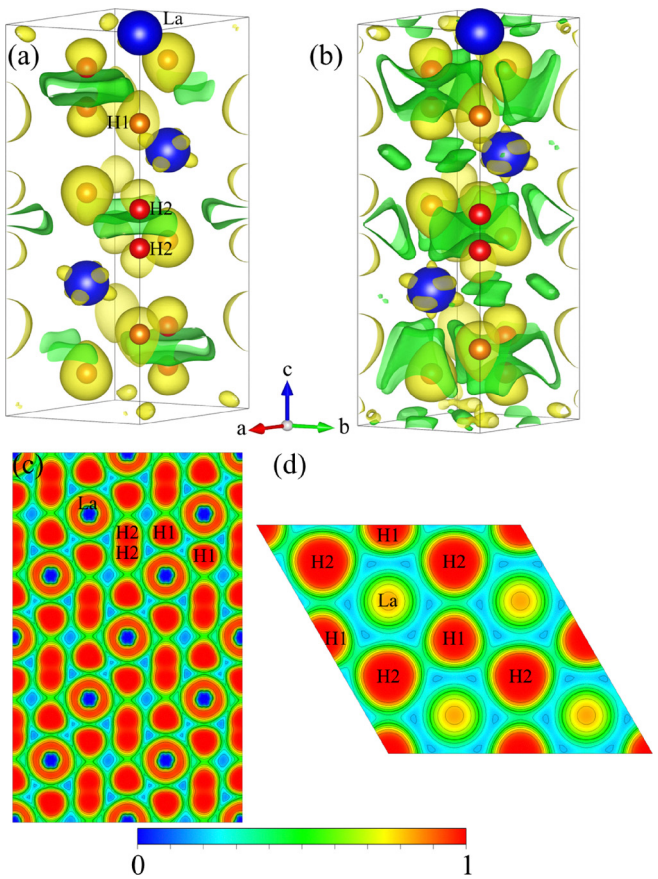

Fig. 4 Charge density difference between the LaH_4 crystal structure and the sum of its constituent atoms at (a) 25 GPa and (b) 100 GPa. The yellow and green colors represent charge accumulation and depletion regions, respectively, with an isosurface value set to 7 × 10^{-2} e Å^{-3}. Electron localization function (ELF) for LaH_4 at 25 GPa taken along the (c) (1 1 0) and (d) (0 0 1) Miller planes, respectively, with a contour spacing set to 0.1. All plots were generated with VESTA.[47]

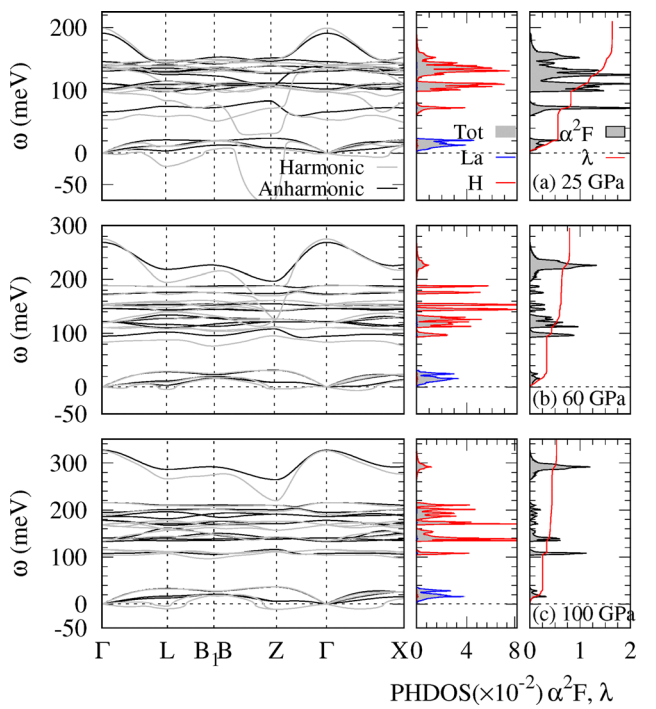

Fig. 5 (a)–(c) Harmonic and anharmonic phonon dispersion, phonon density of states (PHDOS), isotropic Eliashberg spectral function (α^2F), and electron–phonon coupling strength (λ) of LaH_4 at 25, 60, and 100 GPa, respectively. The total PHDOS is decomposed with respect to the vibrations of H (red) and La (blue) atoms. The anharmonic phonon dispersions were computed for a temperature of 300 K.

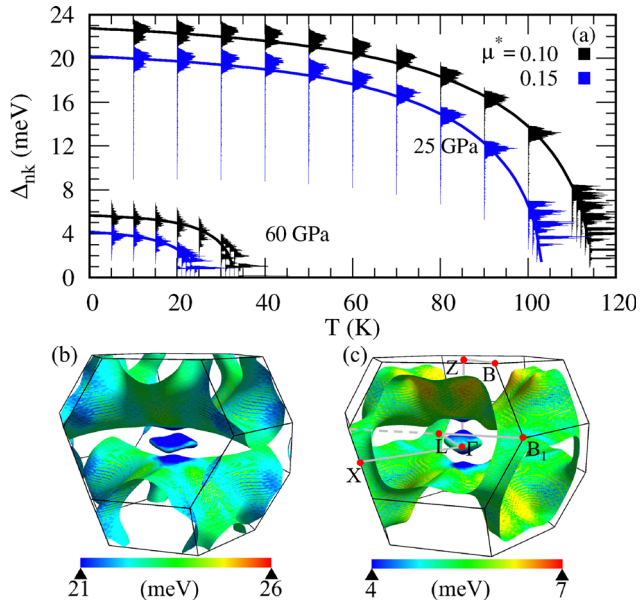

Fig. 6 (a) Histograms of the energy-dependent distribution of the superconducting gap Δ_{nk} as a function of temperature in LaH_4 at 25 and 60 GPa with μ^* = 0.10 (black) and μ^* = 0.15 (blue). The solid lines are guides to the eye. (b) and (c) Momentum-resolved superconducting gap on the Fermi surface in LaH_4 at 25 and 60 GPa with μ^* = 0.10, generated with FermiSurfer.[67]

The acoustic modes arise solely from the vibration of the La atoms, while the intermediate- and high-frequency modes originate exclusively from the motion of the H atoms. From the comparison of the Eliashberg spectral function (α^2F) and the phonon density of states (PHDOS) in the middle and right panels of Fig. 5, we can see that most of the e–ph coupling comes from the hydrogen phonon modes. At 25 GPa, for example, 66% of the total e–ph coupling constant λ of 1.64 comes from the H modes. This λ value is comparable to those computed for LaH_{10} (1.78 and 1.86 at 300 GPa[15,19]) and La_4H_{23} (1.49 at 100 GPa[72]), and almost four times larger than that of a predicted tetragonal LaH_4 phase (0.43 at 300 GPa[15]). As pressure increases, the phonon frequencies harden across all regions, and the DOS at the Fermi level decreases. These combined effects lead to a reduction in λ, with values of 0.79 and 0.53 at 60 GPa and 100 GPa, respectively. A similar pressure dependence has been observed in LaH_{10} and La_4H_{23} superconductors.[3,15,29]

To understand the superconducting properties, we solved the anisotropic full-bandwidth Migdal–Eliashberg equations for a Coulomb parameter μ^* in the 0.10–0.20 range, consistent with values used in other studies on superconductivity in lanthanum hydrides.[15,19,29] Fig. 6 presents the energy distribution of the superconducting gap, Δ_{nk}, as a function of temperature along with its momentum-resolved k-dependence on the Fermi surface at select pressure and μ^* values. Our calculations reveal that LaH_4 exhibits a single anisotropic gap, with an estimated T_c^{aME} of 115 K for μ^* = 0.10 at 25 GPa. In comparison, the McMillan (McM) equation,[73] the Allen–Dynes (AD) formula,[74] the machine-learned (ML) SISSO model,[75] and the isotropic Migdal–Eliashberg (iME) formalism yield T_c^{McM} = 72.5 K, T_c^{AD} = 85.4 K, T_c^{ML} = 102.7 K, and T_c^{iME} = 117 K, respectively. To put this into context, T_c^{iME} was predicted to be 254 K at 300 GPa in LaH_{10},[15] 95 K at 100 GPa in La_4H_{23},[29] and only 10 K at 300 GPa in a tetragonal LaH_4 phase[15] for μ^* = 0.10. The estimated T_c^{aME} in $R\bar{3}m$-LaH_4 is less than half that of LaH_{10} but slightly higher than that in La_4H_{23}, and more importantly, it could be achieved at significantly lower pressures than in these cases. The critical temperature decreases significantly with pressure, with T_c^{aME} dropping to 33 K at 60 GPa and 14 K at 100 GPa. Results for different μ^* values and various approaches for calculating the critical temperature are summarized in Table 2.

As mentioned above, the rapid decrease in T_c with increasing pressure can be directly attributed to a reduction in the DOS at the Fermi level and the hardening of the phonon frequencies. Delving deeper, superconducting hydrides are designed to provide a lattice that promotes the dissociation of molecular H_2, facilitating the formation of metallic hydrogen under pressure.[13] Consequently, a reduction in the H–H distance within the H_2 units may suppress superconductivity, aligning with our observations. As summarized in Table 1, the highest T_c of 115 K is achieved at 25 GPa, where the shortest H–H distance is d_{H-H} = 0.96 Å. However, T_c drops sharply as pressure increases, reaching just 11 K at 100 GPa where d_{H-H} = 0.88 Å. For reference, the bond length of a H_2 molecule is approximately 0.74 Å,[76] while the H–H distance in metallic hydrogen is predicted to be around 1 Å at 500 GPa.[65] This trend, along with the increased charge depletion between the H_2 units at higher pressures, suggests that hydrogen may transition toward a

Table 2 Properties of LaH_4 at 25, 60, and 100 GPa: density of states at the Fermi level (N_F), logarithmic average phonon frequency (ω_{log}), total electron–phonon coupling strength (λ), semiempirical Coulomb parameter (μ^*), and superconducting critical temperature (T_c). The T_c values are calculated using different methodologies: McMillan equation (T_c^{AD}), Allen–Dynes formula (T_c^{AD}), machine-learned SISSO mode (T_c^{ML}), isotropic Migdal–Eliashberg formalism (T_c^{iME}), and anisotropic Migdal–Eliashberg formalism (T_c^{aME})

Pressure (GPa)	N_F (states per eV f.u.$^{-1}$)	ω_{log} (meV)	λ	μ^*	T_c^{McM} (K)	T_c^{AD} (K)	T_c^{ML} (K)	T_c^{iME} (K)	T_c^{aME} (K)
25	0.81	50.6	1.64	0.10	72.5	85.4	102.7	117	115
				0.15	62.8	71.5	85.1	103	102
				0.20	53.1	59.1	68.7	93	92
60	0.54	48.7	0.79	0.10	26.0	27.4	25.3	29	34
				0.15	17.8	18.6	16.2	21	24
				0.20	10.9	11.2	10.3	16	15
100	0.44	56.1	0.53	0.10	9.8	10.1	7.3	9	11
				0.15	4.4	4.5	3.0	9	9
				0.20	1.3	1.3	0.9	—	6

molecular H_2-like state rather than a metallic phase under compression.

4 Conclusion

We carried out an *ab initio* study to explore the superconducting potential of a new low-pressure rhombohedral LaH_4 phase. Our results show that the inclusion of anharmonic corrections is crucial for stabilizing the crystal structure, highlighting the importance of these effects when investigating lanthanum hydrides under pressure. Furthermore, we find that the superconducting temperature can reach up to 115 K at 25 GPa but decreases rapidly with increasing pressure, a common trend in hydride superconductors. Besides experimentally confirming superconductivity of the rhombohedral phase in the 25–100 GPa range, it would be interesting to explore whether this phase could be stabilized down to ambient pressure. These results are exciting as they contribute to the ongoing search for hydrogen-rich compounds capable of achieve high-temperature superconductivity at lower pressures.

Conflicts of interest

There are no conflicts to declare.

Data availability

The data supporting this article is included in the manuscript.

Supplementary information is available. See DOI: **https://doi.org/10.1039/d5tc02600h**.

Acknowledgements

We would like to thank Dr. Vitalie Stavila for useful discussions. C. R. and E. R. M. acknowledge support from the National Science Foundation (NSF) under award no. DMR-2035518. This work used the Frontera supercomputer at the Texas Advanced Computing Center *via* the Leadership Resource Allocation (LRAC) award DMR22004 and the Expanse system at the San Diego Supercomputer Center through the ACCESS allocation TG-DMR180071. M. Z. acknowledges funding by the European Union (project ULTRA-2DPK/HORIZON-MSCA-2022-PF-01/ grant agreement no. 101106654) and computational resources from the EuroHPC Joint Undertaking and supercomputer LUMI **https://lumi-supercomputer.eu/**, hosted by CSC (Finland) and the LUMI consortium through a EuroHPC Extreme Scale Access call. Sandia National Laboratories is a multimission laboratory managed and operated by National Technology and Engineering Solutions of Sandia, LLC, a wholly owned subsidiary of Honeywell International, Inc., for the U.S. Department of Energy (DOE)'s National Nuclear Security Administration under contract no. DE-NA-0003525. The views expressed in the article do not necessarily represent the views of the U.S. DOE or the U.S. Government. The XRD work was performed on APS beam time award from the Advanced Photon Source, a U.S. DOE Office of Science user facility operated for the DOE Office of Science by Argonne National Laboratory under contract no. DE-AC02-06CH11357. HPCAT operations are supported by DOE-NNSA's Office of Experimental Sciences.

References

1 A. P. Drozdov, M. I. Eremets, I. A. Troyan, V. Ksenofontov and S. I. Shylin, Conventional superconductivity at 203 kelvin at high pressures in the sulfur hydride system, *Nature*, 2015, **525**, 73.

2 M. Somayazulu, M. Ahart, A. K. Mishra, Z. M. Geballe, M. Baldini, Y. Meng, V. V. Struzhkin and R. J. Hemley, Evidence for Superconductivity above 260 K in Lanthanum Superhydride at Megabar Pressures, *Phys. Rev. Lett.*, 2019, **122**, 027001.

3 A. P. Drozdov, P. P. Kong, V. S. Minkov, S. P. Besedin, M. A. Kuzovnikov, S. Mozaffari, L. Balicas, F. F. Balakirev, D. E. Graf, V. B. Prakapenka, E. Greenberg, D. A. Knyazev, M. Tkacz and M. I. Eremets, Superconductivity at 250 K in lanthanum hydride under high pressures, *Nature*, 2019, **569**, 528.

4 P. P. Kong, V. S. Minkov, M. A. Kuzovnikov, S. P. Besedin, A. P. Drozdov, S. Mozaffari, L. Balicas, F. F. Balakirev, V. B. Prakapenka, E. Greenberg, D. A. Knyazev and M. I. Eremets, Superconductivity up to 243 K in yttrium hydrides under high pressure, *Nat. Commun.*, 2021, **12**, 5075.

5 A. V. Troyan, A. O. Lyakhov, A. O. Kurnosov, I. A. Abrikosov, A. O. Shorikov, A. O. Ivanovskii, A. V. Baranov and A. V. Chulkov, Anomalous High-Temperature Superconductivity in YH6, *Adv. Mater.*, 2021, **33**, 2006832.

6 Z. Li, X. He, C. Zhang, X. Wang, S. Zhang, Y. Jia, S. Feng, K. Lu, J. Zhao, J. Zhang, B. Min, Y. Long, R. Yu, L. Wang, M. Ye, Z. Zhang, V. Prakapenka, S. Chariton, P. A. Ginsberg, J. Bass, S. Yuan, H. Liu and C. Jin, Superconductivity above 200 K discovered in superhydrides of calcium, *Nat. Commun.*, 2022, **13**, 2863.

7 L. Ma, K. Wang, Y. Xie, X. Yang, Y. Wang, M. Zhou, H. Liu, X. Yu, Y. Zhao, H. Wang, G. Liu and Y. Ma, High-Temperature Superconducting Phase in Clathrate Calcium Hydride CaH6 up to 215 K at a Pressure of 172 GPa, *Phys. Rev. Lett.*, 2022, **128**, 167001.

8 N. P. Salke, M. M. Davari Esfahani, Y. Zhang, I. A. Kruglov, J. Zhou, Y. Wang, E. Greenberg, V. B. Prakapenka, J. Liu, A. R. Oganov and J.-F. Lin, Synthesis of clathrate cerium superhydride CeH9 at 80–100 GPa with atomic hydrogen sublattice, *Nat. Commun.*, 2019, **10**, 4453.

9 W. Chen, D. V. Semenok, X. Huang, H. Shu, X. Li, D. Duan, T. Cui and A. R. Oganov, High-Temperature Superconducting Phases in Cerium Superhydride with a T_c up to 115 K below a Pressure of 1 Megabar, *Phys. Rev. Lett.*, 2021, **127**, 117001.

10 Z.-Y. Cao, S. Choi, L.-C. Chen, P. Dalladay-Simpson, H. Jang, F. A. Gorelli, J.-F. Yan, S.-G. Jung, G. Huang, L. Yu, Y. Lee, J. Kim, T. Park and X.-J. Chen, *Probing superconducting gap in CeH_9 under pressure*, *arXiv*, 2024, preprint, arXiv:2401.12682 cond-mat.supr-con, DOI: **10.48550/arXiv.2401.1268**.

11 D. V. Semenok, A. G. Kvashnin, A. G. Ivanova, V. Svitlyk, V. Y. Fominski, A. V. Sadakov, O. A. Sobolevskiy, V. M. Pudalov, I. A. Troyan and A. R. Oganov, Superconductivity at 161 K in thorium hydride ThH10: Synthesis and properties, *Mater. Today*, 2020, **33**, 36.
12 I. A. Wrona, P. Niegodajew and A. P. Durajski, A recipe for an effective selection of promising candidates for high-temperature superconductors among binary hydrides, *Mater. Today Phys.*, 2024, **46**, 101499.
13 N. W. Ashcroft, Hydrogen Dominant Metallic Alloys: High Temperature Superconductors?, *Phys. Rev. Lett.*, 2004, **92**, 187002.
14 Z. M. Geballe, H. Liu, A. K. Mishra, M. Ahart, M. Somayazulu, Y. Meng, M. Baldini and R. J. Hemley, Synthesis and stability of lanthanum superhydrides, *Angew. Chem., Int. Ed.*, 2018, **57**, 688.
15 H. Liu, I. I. Naumov, R. Hoffmann, N. W. Ashcroft and R. J. Hemley, Potential high-T_c superconducting lanthanum and yttrium hydrides at high pressure, *Proc. Natl. Acad. Sci. U. S. A.*, 2017, **114**, 6990.
16 H. Liu, I. I. Naumov, Z. M. Geballe, M. Somayazulu, J. S. Tse and R. J. Hemley, Dynamics and superconductivity in compressed lanthanum superhydride, *Phys. Rev. B*, 2018, **98**, 100102.
17 D. Sun, V. S. Minkov, S. Mozaffari, Y. Sun, Y. Ma, S. Chariton, V. B. Prakapenka, M. I. Eremets, L. Balicas and F. F. Balakirev, High-temperature superconductivity on the verge of a structural instability in lanthanum superhydride, *Nat. Commun.*, 2021, **12**, 6863.
18 I. Errea, F. Belli, L. Monacelli, A. Sanna, T. Koretsune, T. Tadano, R. Bianco, M. Calandra, R. Arita, F. Mauri and J. A. Flores-Livas, Quantum crystal structure in the 250-kelvin superconducting lanthanum hydride, *Nature*, 2020, **578**, 66.
19 C. Wang, S. Yi and J.-H. Cho, Multiband nature of room-temperature superconductivity in LaH_{10} at high pressure, *Phys. Rev. B*, 2020, **101**, 104506.
20 Y. L. Wu, X. H. Yu, J. Z. L. Hasaien, F. Hong, P. F. Shan, Z. Y. Tian, Y. N. Zhai, J. P. Hu, J. G. Cheng and J. Zhao, Ultrafast dynamics evidence of strong coupling superconductivity in $LaH_{10} \pm \delta$, *Nat. Commun.*, 2024, **15**, 9683.
21 Z. Wu, Y. Sun, A. P. Durajski, F. Zheng, V. Antropov, K.-M. Ho and S. Wu, Effect of doping on the phase stability and superconductivity in LaH_{10}, *Phys. Rev. Mater.*, 2023, **7**, L101801.
22 M. Caussé, G. Geneste and P. Loubeyre, Superionicity of $H^{\delta-}$ in LaH_{10} superhydride, *Phys. Rev. B*, 2023, **107**, L060301.
23 K. K. Ly and D. M. Ceperley, Stability and distortion of fcc LaH_{10} with path-integral molecular dynamics, *Phys. Rev. B*, 2022, **106**, 054106.
24 Y. Watanabe, T. Nomoto and R. Arita, Quantum and temperature effects on the crystal structure of superhydride LaH_{10}: A path integral molecular dynamics study, *Phys. Rev. B*, 2022, **105**, 174111.
25 X. Liang, A. Bergara, X. Wei, X. Song, L. Wang, R. Sun, H. Liu, R. J. Hemley, L. Wang, G. Gao and Y. Tian, Prediction of high-T_c superconductivity in ternary lanthanum borohydrides, *Phys. Rev. B*, 2021, **104**, 134501.
26 A. K. Verma, P. Modak, F. Schrodi, A. Aperis and P. M. Oppeneer, Prediction of an unusual trigonal phase of superconducting LaH_{10} stable at high pressures, *Phys. Rev. B*, 2021, **104**, 174506.
27 Y. Ge, F. Zhang and R. J. Hemley, Room-temperature superconductivity in boron- and nitrogen-doped lanthanum superhydride, *Phys. Rev. B*, 2021, **104**, 214505.
28 D. Laniel, F. Trybel, B. Winkler, F. Knoop, T. Fedotenko, S. Khandarkhaeva, A. Aslandukova, T. Meier, S. Chariton, K. Glazyrin, V. Milman, V. Prakapenka, I. A. Abrikosov, L. Dubrovinsky and N. Dubrovinskaia, High-pressure synthesis of seven lanthanum hydrides with a significant variability of hydrogen content, *Nat. Commun.*, 2022, **13**, 6987.
29 J. Guo, D. Semenok, G. Shutov, D. Zhou, S. Chen, Y. Wang, K. Zhang, X. Wu, S. Luther, T. Helm, X. Huang and T. Cui, Unusual metallic state in superconducting A15-type La4H23, *Natl. Sci. Rev.*, 2024, **11**, nwae149.
30 S. Cross, J. Buhot, A. Brooks, W. Thomas, A. Kleppe, O. Lord and S. Friedemann, High-temperature superconductivity in La_4H_{23} below 100 GPa, *Phys. Rev. B*, 2024, **109**, L020503.
31 S. Duwal, V. Stavila, C. Spataru, M. Shivanna, P. Allen, T. Elmslie, C. T. Seagle, J. Jeffries, N. Velisavljevic, J. Smith, P. Chow, Y. Xiao, M. Somayazulu and P. A. Sharma, *Enhancement of hydrogen absorption and hypervalent metal hydride formation in lanthanum using cryogenic ball milling*, *arXiv*, 2025, preprint, arXiv:2506.23980, DOI: **10.48550/arXiv.2506.23980**.
32 P. Giannozzi, S. Baroni, N. Bonini, M. Calandra, R. Car, C. Cavazzoni, D. Ceresoli, G. L. Chiarotti, M. Cococcioni, I. Dabo, A. D. Corso, S. de Gironcoli, S. Fabris, G. Fratesi, R. Gebauer, U. Gerstmann, C. Gougoussis, A. Kokalj, M. Lazzeri, L. Martin-Samos, N. Marzari, F. auri, R. Mazzarello, S. Paolini, A. Pasquarello, L. Paulatto, C. Sbraccia, S. Scandolo, G. Sclauzero, A. P. Seitsonen, A. Smogunov, P. Umari and R. M. Wentzcovitch, QUANTUM ESPRESSO: a modular and opensource software project for quantum simulations of materials, *J. Phys.: Condens. Matter*, 2009, **21**, 395502.
33 P. Giannozzi, O. Andreussi, T. Brumme, O. Bunau, M. B. Nardelli, M. Calandra, R. Car, C. Cavazzoni, D. Ceresoli, M. Cococcioni, N. Colonna, I. Carnimeo, A. D. Corso, S. de Gironcoli, P. Delugas, R. A. DiStasio, A. Ferretti, A. Floris, G. Fratesi, G. Fugallo, R. Gebauer, U. Gerstmann, F. Giustino, T. Gorni, J. Jia, M. Kawamura, H.-Y. Ko, A. Kokalj, E. Küçükbenli, M. Lazzeri, M. Marsili, N. Marzari, F. Mauri, N. L. Nguyen, H.-V. Nguyen, A. O. de-la Roza, L. Paulatto, S. Poncé, D. Rocca, R. Sabatini, B. Santra, M. Schlipf, A. P. Seitsonen, A. Smogunov, I. Timrov, T. Thonhauser, P. Umari, N. Vast, X. Wu and S. Baroni, Advanced capabilities for materials modelling with Quantum ESPRESSO, *J. Phys.: Condens. Matter*, 2017, **29**, 465901.
34 D. R. Hamann, Optimized norm-conserving Vanderbilt pseudopotentials, *Phys. Rev. B: Condens. Matter Mater. Phys.*, 2013, **88**, 085117.

35 M. van Setten, M. Giantomassi, E. Bousquet, M. Verstraete, D. Hamann, X. Gonze and G.-M. Rignanese, The PseudoDojo: Training and grading a 85 element optimized norm-conserving pseudopotential table, *Comput. Phys. Commun.*, 2018, **226**, 39.

36 J. P. Perdew, A. Ruzsinszky, G. I. Csonka, O. A. Vydrov, G. E. Scuseria, L. A. Constantin, X. Zhou and K. Burke, Restoring the Density-Gradient Expansion for Exchange in Solids and Surfaces, *Phys. Rev. Lett.*, 2008, **100**, 136406.

37 H. J. Monkhorst and J. D. Pack, Special points for Brillouin-zone integrations, *Phys. Rev. B*, 1976, **13**, 5188.

38 M. Methfessel and A. T. Paxton, High-precision sampling for Brillouin-zone integration in metals, *Phys. Rev. B: Condens. Matter Mater. Phys.*, 1989, **40**, 3616.

39 S. Baroni, S. de Gironcoli, A. Dal Corso and P. Giannozzi, Phonons and related crystal properties from density-functional perturbation theory, *Rev. Mod. Phys.*, 2001, **73**, 515.

40 M. Zacharias and F. Giustino, One-shot calculation of temperature-dependent optical spectra and phononinduced band-gap renormalization, *Phys. Rev. B*, 2016, **94**, 075125.

41 M. Zacharias and F. Giustino, Theory of the special displacement method for electronic structure calculations at finite temperature, *Phys. Rev. Res.*, 2020, **2**, 013357.

42 M. Zacharias, G. Volonakis, F. Giustino and J. Even, Anharmonic lattice dynamics via the special displacement method, *Phys. Rev. B*, 2023, **108**, 035155.

43 N. R. Werthamer, Self-consistent phonon formulation of anharmonic lattice dynamics, *Phys. Rev. B*, 1970, **1**, 572.

44 H. Lee, S. Poncé, K. Bushick, S. Hajinazar, J. Lafuente-Bartolome, J. Leveillee, C. Lian, J.-M. Lihm, F. Macheda, H. Mori, H. Paudyal, W. H. Sio, S. Tiwari, M. Zacharias, X. Zhang, N. Bonini, E. Kioupakis, E. R. Margine and F. Giustino, Electron–phonon physics from first principles using the EPW code, *npj Comput. Mater.*, 2023, **9**, 156.

45 S. B. Mishra, H. Mori and E. R. Margine, *Electronphonon vertex correction effect in superconducting H_3S*, *arXiv*, 2025, preprint, arXiv:2507.01897 cond-mat.supr-con, DOI: **10.48550/arXiv.2507.01897**.

46 See Fig. S1–S3.

47 K. Momma and F. Izumi, VESTA3 for three-dimensional visualization of crystal, volumetric and morphology data, *J. Appl. Crystallogr.*, 2011, **44**, 1272.

48 F. Giustino, M. L. Cohen and S. G. Louie, Electronphonon interaction using Wannier functions, *Phys. Rev. B*, 2007, **76**, 165108.

49 E. R. Margine and F. Giustino, Anisotropic Migdal–Eliashberg theory using Wannier functions, *Phys. Rev. B*, 2013, **87**, 024505.

50 S. Poncé, E. Margine, C. Verdi and F. Giustino, EPW: Electron–phonon coupling, transport and superconducting properties using maximally localizedWannier functions, *Comput. Phys. Commun.*, 2016, **209**, 116.

51 N. Marzari, A. A. Mostofi, J. R. Yates, I. Souza and D. Vanderbilt, Maximally localized Wannier functions: Theory and applications, *Rev. Mod. Phys.*, 2012, **84**, 1419.

52 G. Pizzi, V. Vitale, R. Arita, S. Blügel, F. Freimuth, G. Géranton, M. Gibertini, D. Gresch, C. Johnson, T. Koretsune, J. Ibãnez-Azpiroz, H. Lee, J.-M. Lihm, D. Marchand, A. Marrazzo, Y. Mokrousov, J. I. Mustafa, Y. Nohara, Y. Nomura, L. Paulatto, S. Poncé, T. Ponweiser, J. Qiao, F. Thöle, S. S. Tsirkin, M. Wierzbowska, N. Marzari, D. Vanderbilt, I. Souza, A. A. Mostofi and J. R. Yates, Wannier90 as a community code: new features and applications, *J. Phys.: Condens. Matter*, 2020, **32**, 165902.

53 R. Lucrezi, P. P. Ferreira, S. Hajinazar, H. Mori, H. Paudyal, E. R. Margine and C. Heil, Full-bandwidth anisotropic Migdal–Eliashberg theory and its application to superhydrides, *Commun. Phys.*, 2024, **7**, 33.

54 H. Mori, T. Nomoto, R. Arita and E. R. Margine, Efficient anisotropic Migdal–Eliashberg calculations with an intermediate representation basis and Wannier interpolation, *Phys. Rev. B*, 2024, **110**, 064505.

55 V. Stavila, S. Li, C. Dun, M. A. T. Marple, H. E. Mason, J. L. Snider, J. E. r Reynolds, F. El Gabaly, J. D. Sugar, C. D. Spataru, X. Zhou, B. Dizdar, E. H. Majzoub, R. Chatterjee, J. Yano, H. Schlöombeg, B. V. Lotsch, J. J. Urban, B. C. Wood and M. D. Allendorf, Defying Thermodynamics: Stabilization of Alane Within Covalent Triazine Frameworks for Reversible Hydrogen Storage, *Angew. Chem., Int. Ed.*, 2021, **60**, 25815.

56 F. Peng, Y. Sun, C. J. Pickard, R. J. Needs, Q. Wu and Y. Ma, Hydrogen Clathrate Structures in Rare Earth Hydrides at High Pressures: Possible Route to Room-Temperature Superconductivity, *Phys. Rev. Lett.*, 2017, **119**, 107001.

57 P. Kong, V. S. Minkov, M. A. Kuzovnikov, A. P. Drozdov, S. P. Besedin, S. Mozaffari, L. Balicas, F. F. Balakirev, V. B. Prakapenka, S. Chariton, D. A. Knyazev, E. Greenberg and M. I. Eremets, Superconductivity up to 243 K in the yttrium-hydrogen system under high pressure, *Nat. Commun.*, 2021, **12**, 5075.

58 Y. Li, J. Hao, H. Liu, J. S. Tse, Y. Wang and Y. Ma, Pressure-stabilized superconductive yttrium hydrides, *Sci. Rep.*, 2015, **5**, 9948.

59 X. Feng, J. Zhang, G. Gao, H. Liu and H. Wang, Compressed sodalite-like mgh6 as a potential hightemperature superconductor, *RSC Adv.*, 2015, **5**, 59292.

60 J. Zhao, B. Ao, S. Li, T. Gao and X. Ye, Phase Diagram and Bonding States of Pu–H Binary Compounds at High Pressures, *J. Phys. Chem. C*, 2020, **124**, 7361.

61 Y.-L. Hai, N. Lu, H.-L. Tian, M.-J. Jiang, W. Yang, W.-J. Li, X.-W. Yan, C. Zhang, X.-J. Chen and G.-H. Zhong, Cage Structure and Near Room-Temperature Superconductivity in TbH*n* (*n* = 1–12), The, *J. Phys. Chem. C*, 2021, **125**, 3640.

62 D. V. Semenok, D. Zhou, A. G. Kvashnin, X. Huang, M. Galasso, I. A. Kruglov, A. G. Ivanova, A. G. Gavriliuk, W. Chen, N. V. Tkachenko, A. I. Boldyrev, I. Troyan, A. R. Oganov and T. Cui, Novel Strongly Correlated Europium Superhydrides, The, *J. Phys. Chem. Lett.*, 2021, **12**, 32.

63 W. Sun, X. Kuang, H. D. J. Keen, C. Lu and A. Hermann, Second group of high-pressure high-temperature lanthanide polyhydride superconductors, *Phys. Rev. B*, 2020, **102**, 144524.

64 X. Zhong, H. Wang, J. Zhang, H. Liu, S. Zhang, H.-F. Song, G. Yang, L. Zhang and Y. Ma, Tellurium hydrides at high pressures: High-temperature superconductors, *Phys. Rev. Lett.*, 2016, **116**, 057002.
65 N. W. Ashcroft, Metallic Hydrogen: A High-Temperature Superconductor?, *Phys. Rev. Lett.*, 1968, **21**, 1748.
66 H. W. T. Morgan and A. N. Alexandrova, Structures of LaH_{10}, EuH_9, and UH_8 superhydrides rationalized by electron counting and Jahn–Teller distortions in a covalent cluster model, *Chem. Sci.*, 2023, **14**, 6679.
67 M. Kawamura, Fermisurfer: Fermi-surface viewer providing multiple representation schemes, *Comput. Phys. Commun.*, 2019, **239**, 197.
68 I. Errea, M. Calandra and F. Mauri, First-principles theory of anharmonicity and the inverse isotope effect in superconducting palladium-hydride compounds, *Phys. Rev. Lett.*, 2013, **111**, 177002.
69 I. Errea, M. Calandra, C. J. Pickard, J. Nelson, R. J. Needs, Y. Li, H. Liu, Y. Zhang, Y. Ma and F. Mauri, High-pressure hydrogen sulfide from first principles: A strongly anharmonic phonon-mediated superconductor, *Phys. Rev. Lett.*, 2015, **114**, 157004.
70 P. Hou, F. Belli, R. Bianco and I. Errea, Quantum anharmonic enhancement of superconductivity in *P*63/*mmc* ScH6 at high pressures: A first-principles study, *J. Appl. Phys.*, 2021, **130**, 175902.
71 M. Dogan, S. Oh and M. L. Cohen, High temperature superconductivity in the candidate phases of solid hydrogen, *J. Phys.: Condens. Matter*, 2022, **34**, 15LT01.
72 J. J. Gilman, Lithium Dihydrogen Fluoride—An Approach to Metallic Hydrogen, *Phys. Rev. Lett.*, 1971, **26**, 546.
73 W. L. McMillan, Transition temperature of strongcoupled superconductors, *Phys. Rev.*, 1968, **167**, 331.
74 P. B. Allen and R. C. Dynes, Transition temperature of strong-coupled superconductors reanalyzed, *Phys. Rev. B*, 1975, **12**, 905.
75 S. R. Xie, G. R. Stewart, J. J. Hamlin, P. J. Hirschfeld and R. G. Hennig, Functional form of the superconducting critical temperature from machine learning, *Phys. Rev. B*, 2019, **100**, 174513.
76 K. P. Huber and G. Herzberg, Constants of diatomic molecules, *Molecular Spectra and Molecular Structure: IV. Constants of Diatomic Molecules*, Springer, US, Boston, MA, 1979, pp. 8–689.